The optimal antenna for nonlinear spectroscopy of weakly and strongly scattering nanoobjects

Thorsten Schumacher[1,2,3] · Matthias Brandstetter[1,2,3] · Daniela Wolf[1,2,3] ·
Kai Kratzer[2,3] · Mario Hentschel[2,3] · Harald Giessen[3] · Markus Lippitz[1,2,3]

Abstract Optical nanoantennas, i.e., arrangements of plasmonic nanostructures, promise to enhance the light–matter interaction on the nanoscale. In particular, nonlinear optical spectroscopy of single nanoobjects would profit from such an antenna, as nonlinear optical effects are already weak for bulk material, and become almost undetectable for single nanoobjects. We investigate the design of optical nanoantennas for transient absorption spectroscopy in two different cases: the mechanical breathing mode of a metal nanodisk and the quantum-confined carrier dynamics in a single CdSe nanowire. In the latter case, an antenna with a resonance at the desired wavelength optimally increases the light intensity at the nanoobject. In the first case, the perturbation of the antenna by the investigated nanosystem cannot be neglected and off-resonant antennas become most efficient.

This article is part of the topical collection "Ultrafast Nanooptics" guest edited by Martin Aeschlimann and Walter Pfeiffer.

✉ Thorsten Schumacher
thorsten.schumacher@uni-bayreuth.de

Markus Lippitz
markus.lippitz@uni-bayreuth.de

[1] Experimental Physics III, University of Bayreuth, Universitätsstrasse 30, 95440 Bayreuth, Germany

[2] Max Planck Institute for Solid State Research, Heisenbergstrasse 1, 70569 Stuttgart, Germany

[3] 4th Physics Institute and Research Center SCoPE, University of Stuttgart, Pfaffenwaldring 57, 70550 Stuttgart, Germany

1 Introduction

Semiconductor and metal nanoparticles of a few nanometers in size show exceptional linear and nonlinear optical behavior [1, 2], which make them very appealing nanosystems for fundamental research and future technologies. However, their investigation and utilization are complicated by their tiny interaction cross sections with light. Optical nanoantennas composed of plasmonic nanoparticles bridge the gap between individual nanoscopic systems and the outside world, thus giving access to previously unattainable dimensions in nanospace [3, 4]. Many fascinating experiments have demonstrated the potential of optical nanoantennas. Examples range from coherent nonlinear optics, where the higher harmonics generation is boosted within the antenna itself [5–8], to local probes for sensing applications [9], increased emission and excitation efficiency of emitters [10, 11], and enhanced nonlinear response of a single nanosystem [12]. However, particle plasmons can be tuned via many different parameters that offer many degrees of freedom [13, 14]. In order to achieve the highest efficiency, the antenna has to be crucially optimized to match the requirements of the experimental method and the nanosystem under investigation.

In this article, we discuss the optimum parameters of an optical antenna for ultrafast nonlinear spectroscopy and how the investigated nanosystem itself affects the properties of the most efficient nanoantenna. We distinguish between two cases in which the investigated nanosystem varies in dipole moment and scattering strength. After a brief introduction to the experimental technique of ultrafast nonlinear spectroscopy, a simple model based on the discrete dipole approximation (DDA) will be introduced, which gives insight into the influence of the nanosystem on the antenna. Dependent on the resonance energy and oscillator strength of the
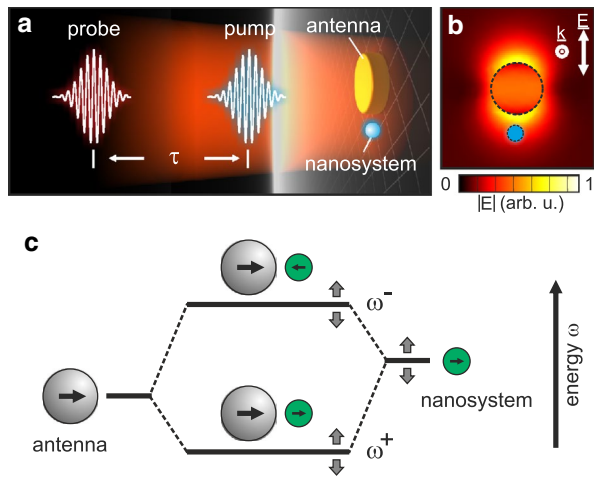
Fig. 1 *Functionality of an optical antenna* **a** The pump pulse triggers an optical process and the temporal and spectral dynamics is interrogated by a probe pulse. For both processes, the light–matter interaction is enhanced by the near field of the antenna. **b** Numerical simulations of the absolute value of the antenna's resonantly scattered near field without nanoobject. The characteristic hot spots promise high sensitivity for optical changes in small local areas (illustrated by the blue circle) in close vicinity to the disk-shaped gold antenna (diameter 70 nm, height 30 nm). **c** Antenna and nanoobject are coupled via their near fields, forming a hybrid system with two new hybrid modes and energy levels. Both hybrid modes ω^+ and ω^- show sensitivity to perturbations in the optical properties of the nanosystem, indicated by the *gray arrows*

nanosystem, we obtain a complex relation with the optical properties of the nanoantenna. These findings are supported by our experiments. As example for a strongly scattering nanosystem, we discuss mechanical breathing oscillations in a single gold nanoparticle [15]. This particle shows strong polarizability and its back-action to the antenna cannot be neglected. We introduce a theoretical model beyond the dipole approximation to find the optimum antenna parameters under realistic conditions and demonstrate a signal enhancement by one order of magnitude in our experiment. As a contrasting second example, we discuss the quantum-confined carrier dynamics in a single CdSe nanowire [16]. Here, the weak backscattering to the antenna can be neglected, leading to a strict relation between the plasmonic resonance of the antenna and the exciton transition energy of the semiconductor wire.

2 Optimal antennas for ultrafast nonlinear spectroscopy of individual nanosystems

Ultrafast nonlinear spectroscopy investigates the deviations from linear light–matter interaction with high temporal resolution [15, 17–19]. Figure 1a depicts the essential parts of the experiment. A pump pulse triggers a process in the

nanosystem. The probe pulse interrogates the response as a function of wavelength and time delay τ. For both pulses, the near field of the antenna modifies the light–matter interaction of the nanoparticle. Figure 1b shows the scattered near field of the single antenna without nanoobject, which would distort the field in dependence of its dipole moment and size. We observe the typical hot spots at the ends of the structure, caused by the large surface carrier density of this dipolar mode. As the near field amplitude exceeds the excitation field, such antennas can be considered as local field compressors or nanolenses. As a consequence, the antenna near field offers a small volume (marked by the blue circle in Fig. 1b) of extremely high energy density compared to the excitation field. This can be directly used for excitation enhancement [11]. However, also a perturbation of the optical properties within this high field volume promises high sensitivity for almost any kind of nanosystem.

Nanoantenna and nanoobject under investigation are coupled via their near fields and form a hybrid system with new optical properties, namely new hybrid states and eigenenergies as sketched in Fig. 1c. In consequence, a perturbation of the nanoobject's properties directly influences the hybrid modes. Dependent on the antenna's properties like resonance position, line width and oscillator strength, the signal modulated onto the hybrid modes can be enhanced with respect to the signal of the single nanosystem.

In order to study the interaction between nanoobject and antenna, we introduce a simple model based on dipole–dipole interaction [20]. We assume an incident light field $\mathbf{E}_{\mathrm{inc}}(\omega, \mathbf{r})$ of our probe beam, impinging on the coupled nanoobjects. Based on the method of discrete dipole approximation (DDA), the dipole moment $\mathbf{p}_i$ of a scatterer with polarizability α_i is given by

$$\mathbf{p}_i = \alpha_i \mathbf{E}_{\mathrm{inc}}(\mathbf{r}_i) + \sum_{h \neq i}^{N-1} \alpha_i \mathbf{E}_{\mathrm{scat},h}(\mathbf{r}_i) \quad . \tag{1}$$

The first term describes the interaction with the incident light field and the second term the interaction with the scattered field $\mathbf{E}_{\mathrm{scat},h}(\mathbf{r}_i)$ of $N-1$ other nanoobjects. Since we consider fundamental dipolar modes of nanoparticles in close vicinity, the retardation-free scattered field of dipole h is given by

$$\mathbf{E}_{\mathrm{scat},h}(\mathbf{r}_i) = \frac{1}{4\pi\epsilon_0\epsilon_r} \frac{1}{\Delta r_{i,h}^3} \left(3 \frac{\Delta \mathbf{r}_{i,h} \mathbf{p}_h}{\Delta r_{i,h}^2} \Delta \mathbf{r}_{i,h} - \mathbf{p}_h \right) \tag{2}$$

with $\Delta \mathbf{r}_{i,h}$ being the displacement vector between two particles. In contrast to common DDA, we apply Lorentzian-type polarizabilities

$$\alpha_i = \frac{\Theta_i}{\left(\omega_{0,i}^2 - \omega^2\right) - i\omega\gamma_i} \tag{3}$$

in order to have full control over the peak polarizability Θ_i, resonance energy $\omega_{0,i}$, and line width γ_i of each object.

In the following, we simplify the system to two particles, namely the antenna and the nanosystem, separated by the distance d, and an excitation along the displacement vector. In consequence, the equation system can be reduced to

$$\begin{pmatrix} 1 & -2\zeta \; \alpha_a/d^3 \\ -2\zeta \; \alpha_n/d^3 x & 1 \end{pmatrix} \begin{pmatrix} p_a \\ p_n \end{pmatrix} = E_{inc} \begin{pmatrix} \alpha_a \\ \alpha_n \end{pmatrix} \quad (4)$$

with $\zeta = 1/(4\pi\epsilon_0\epsilon_r)$. By solving the linear equation system, we obtain the frequency-dependent polarizations p_a and p_n of antenna and nanoobject. Furthermore, the extinction cross section is computed to

$$C_{ext} = \frac{4\pi k}{|\mathbf{E}_0|^2} \sum_{i=1}^{2} \text{Im}\left[\mathbf{E}_{inc,i}^* \cdot \mathbf{p}_i\right]. \quad (5)$$

As an example, we consider a coupled nanoparticle–antenna pair, separated by 20 nm (Fig. 2). The resonance energy of antenna and nanoobject is 2.0 and 2.2 eV, respectively. Both have a line width of 0.1 eV. The peak polarizability of the nanoparticle is 10 times smaller than that of the antenna. In the linear spectra, we see the hybridization effect discussed above. In the field of plasmonics, this coupling scheme is known as plasmon hybridization [21]. However, the physical framework is not limited to plasmonics and holds true for other nanosystems.

In general, the perturbation of the linear properties by a nonlinear process is rather complex and obviously depends on the process itself. For simplicity, we assume a tiny increase in the eigenfrequency of the nanoparticle by 0.1 % to study the efficiency of the antenna with unmodified properties. The nonlinear response is computed by the change of the extinction cross section, caused by the pump-induced perturbation. The signal of the bare nanosystem without antenna follows a dispersive line shape at the single nanosystem's resonance (Fig. 2b). In contrast, the nonlinear response of the hybrid system is modulated on the lower energy hybrid mode and increased compared to the response of the single nanosystem. At the same time, the signal at the higher energy mode is decreased. As expected, the amplitude of the nonlinear response depends on the overall oscillator strength and the quality factor of the resonance. Finally, the antenna's efficiency can be expressed by its maximal achieved enhancement, which is computed by the quotient of the maximum absolute nonlinear response of the hybrid system and the single nanoobject. For the given example, we obtain an enhancement factor of approximately 5. This value does not depend on the perturbation strength, as long as its influence does not drastically change the spectral response of the nanoobject.
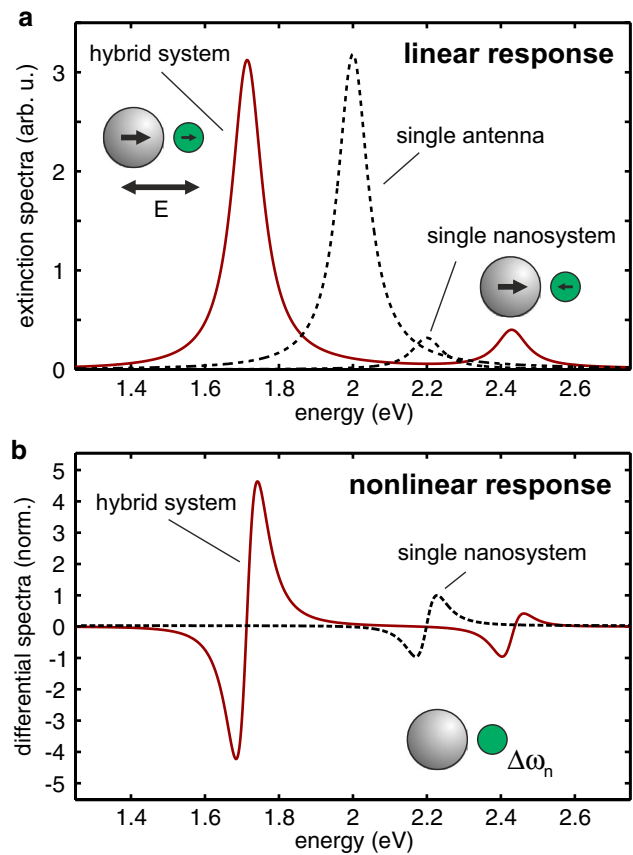

Fig. 2 *Spectral response in the point-dipole model* **a** The hybrid resonances (*red solid curve*) are shifted in energy with respect to their single-particle resonances (*black dashed curve*), as in the plasmon hybridization scheme. The polarizations of the modes are illustrated by the *arrows*. **b** The nonlinear response is computed by a perturbation of the nanosystem's optical properties ($\Delta\omega_n$), leading to a dispersive line shape at the resonances. The normalized signal of the bare nanosystem without antenna (*black dashed curve*) follows a dispersive line shape at the single nanosystem's resonance. The nonlinear response of the hybrid system (*red curve*) is normalized to the maximum response of the single nanoobject

In the following, we employ our model to find the optimum antenna parameters in dependence of the nanoparticle's properties. However, even the two-particle system offers a large parameter space for optimization. Referring to our experimental examples below, we focus on the spectral dependence between optimum antenna and strongly or weakly scattering nanoobject. In consequence, we keep the peak polarizability of antenna and nanoparticle constant while independently tuning their resonance energies. As we use gold nanoantennas, we apply a phenomenological damping parameter γ_a based on the extinction coefficient of gold, calculated from data of Johnson and Christy [22]. The line width of the nanoobject is kept constant at 0.1 eV.

In the case of the strongly scattering nanosystem, its peak polarizability is only one order of magnitude smaller

than the antenna's. Here, the back-action cannot be neglected and detunes the hybrid modes as shown in the previous example. Figure 3a summarizes the maximum signal enhancement for each combination of nanoobject and antenna resonance, extracted from the corresponding full nonlinear spectrum. For better visibility, the enhancement factors are normalized to the best antenna for each nanosystem resonance while the highest achieved enhancement is plotted separately in the lower graph. We obtain values between approximately 4.5 for nanoparticles with their resonance around 1.8 eV and almost no enhancement for nanosystems being resonant at 3 eV. Furthermore, the relation between the resonances of nanosystem and optimum antenna shows a counterintuitive crossing behavior. The red, maximum enhancement region is above the white spectral overlap line for low nanosystem resonance energies. In consequence, the nonlinear response of a nanoparticle at lower energies is most efficiently enhanced by an antenna at higher energies. This reverses for higher energy nanosystem. In between, we find the case at 2.3 eV, where

the optimum antenna and nanosystem are in resonance (the white line crosses the red region). In contrast, the results for the weakly scattering nanoobject show a completely different behavior. Here, its peak polarizability is four orders of magnitude smaller than that of the antenna. Up to approximately 2.3 eV the optimum antenna is resonant to the nanosystem before an off-resonant antenna at around 1.8 eV becomes most efficient, almost independent of the resonance of the nanosystem.

In both cases, the optimum antenna is a compromise of oscillator strength, spectral overlap, and the hybrid mode's resonance. Furthermore, the results are shaped by the dielectric function of the antenna material. The optical properties of gold can be described by a Drude model, matching measured data up to approximately 2.2 eV. At higher energies, the d-band absorption dominates the optical properties, deviating from the simple Drude model of a free electron gas [22]. Consequently, plasmon resonances are strongly damped beyond 2.2 eV. Considering the strongly scattering nanosystem, the hybrid mode resonance
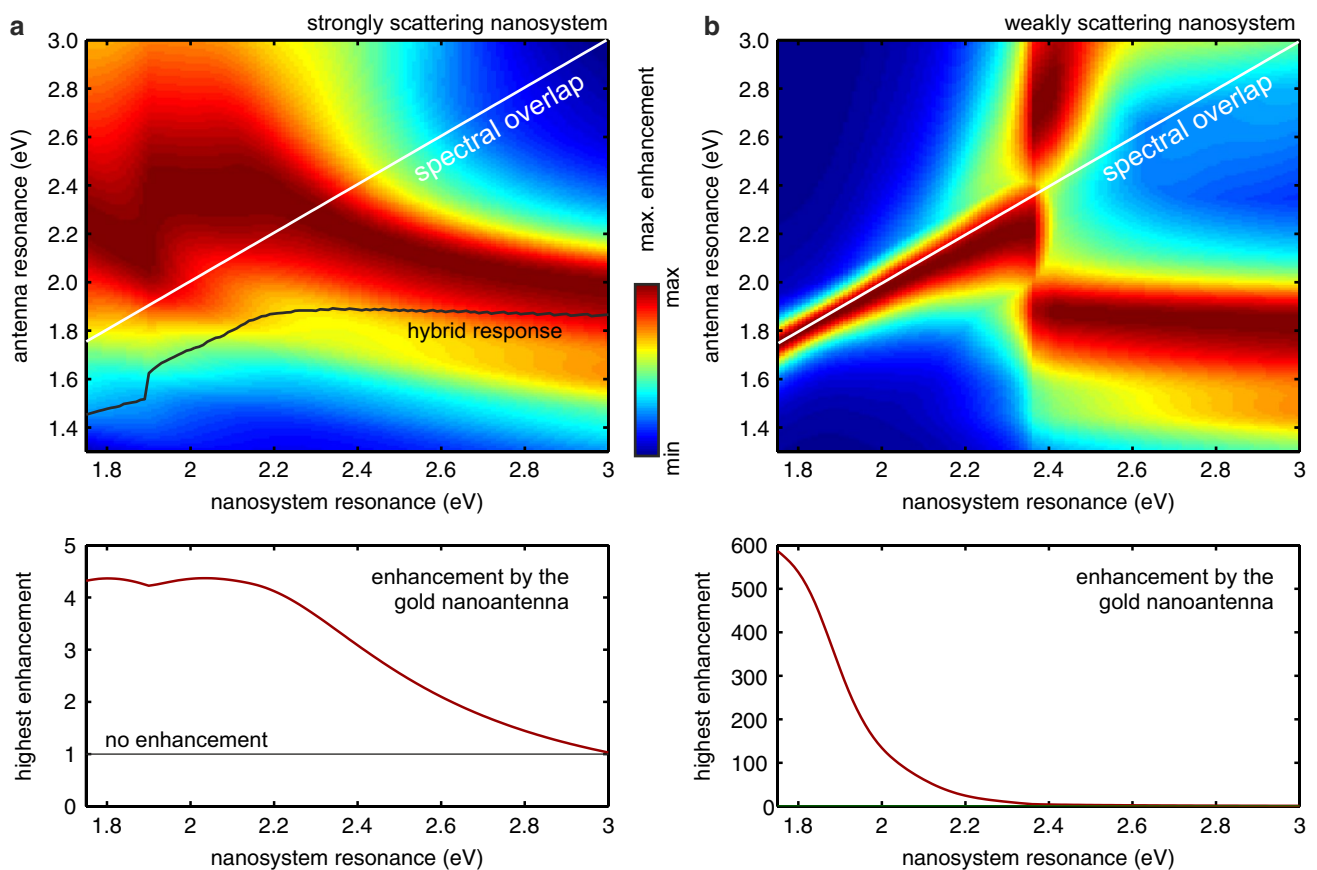

Fig. 3 *Optimum antennas for a strongly and weakly scattering nanosystem* Maximum antenna enhancement for a strongly **a** and a weakly scattering nanosystem **b** as a function of antenna and nanosystem resonance. The enhancement is normalized for each nanosystem resonance energy. The energy of spectral overlap of antenna and nano-object is plotted as *white line*, the hybrid response with the optimum antenna as *black curve*. For the weakly scattering nanoobject, the hybrid response is identical with the antenna resonance. The normalization factor is plotted as highest achieved enhancement in the lower graphs

is detuned with respect to the bare antenna resonance. Dependent on the damping at the hybrid mode's resonance, the nonlinear signal of the nanosystem can be increased but also decreased by an inefficient antenna. Thus, a resonant antenna for nanosystems at lower energies would result in a strong redshift where the hybrid mode is broadened due to the optical properties of gold. A slightly off-resonant antenna at higher energies offers additional dipole moment for the hybrid mode, but still good optical properties and quality factor at its hybrid resonance, plotted as black curve in Fig. 3a. For nanosystems with higher resonance energies, a spectrally overlapping antenna is inefficient due to the d-band absorption and strong damping of the antenna plasmon. Here, an off-resonant antenna at lower energies provides oscillator strength and shifts the hybrid mode outside the d-band absorption. However, the increasing detuning of antenna and nanoparticle decreases the achieved enhancement as shown in the lower graph. In the case of the weakly scattering nanosystem, a resonant antenna shows highest enhancement. Here, the hybrid mode is identical with the bare antenna resonance and no changes in the optical properties have to be considered. The shift of the resonance of the optimum antenna for nanosystems beyond 2.3 eV is simply due to the d-band of gold. Again, an off-resonant antenna is more efficient than a strongly damped resonant antenna. However, the signal enhancement is reduced drastically.

We want to mention again that these results do not depend on the perturbation strength of the nanoparticle's properties. In addition, we find analogous results for other kind of perturbations as, for example, in peak polarizability, damping or any combination. However, in contrast to our model, plasmonic modes cannot be designed that easily. Antenna resonances are geometry but also size dependent and thus correlated via the oscillator strength. In addition, with increasing oscillator strength also the radiative damping of the plasmon is increased, leading to a broadening of the resonance [14]. This complexity opens almost infinite space of optimization, which cannot be considered in a general model. However, the presented study is a first step toward a generalized scheme for optimized antenna design for ultrafast spectroscopy as we show in the following two experimental examples.

3 The optimum antenna for mechanical vibrations in a strongly scattering gold nanoparticle

In the following, we support our model by the example of acoustic vibrations in a strongly scattering single gold nanoparticle. Nanostructures of a few ten nanometers in size can perform mechanical oscillations, still following the laws of continuum mechanics, where the discretized nature

of the material can be neglected [18, 23]. Figure 4a shows a selection of mechanical modes of a disk-shaped gold nanoparticle lying on an inelastic substrate. The computation is done using the structural mechanics module of COMSOL Multiphysics [24]. In order to experimentally investigate these modes, we apply an ultrafast pump-probe technique and measure the transient absorption signal of a single gold nanoparticle [15].

As an example, we choose the diameter to 70 nm and height to 30 nm at an excitation wavelength of 800 nm
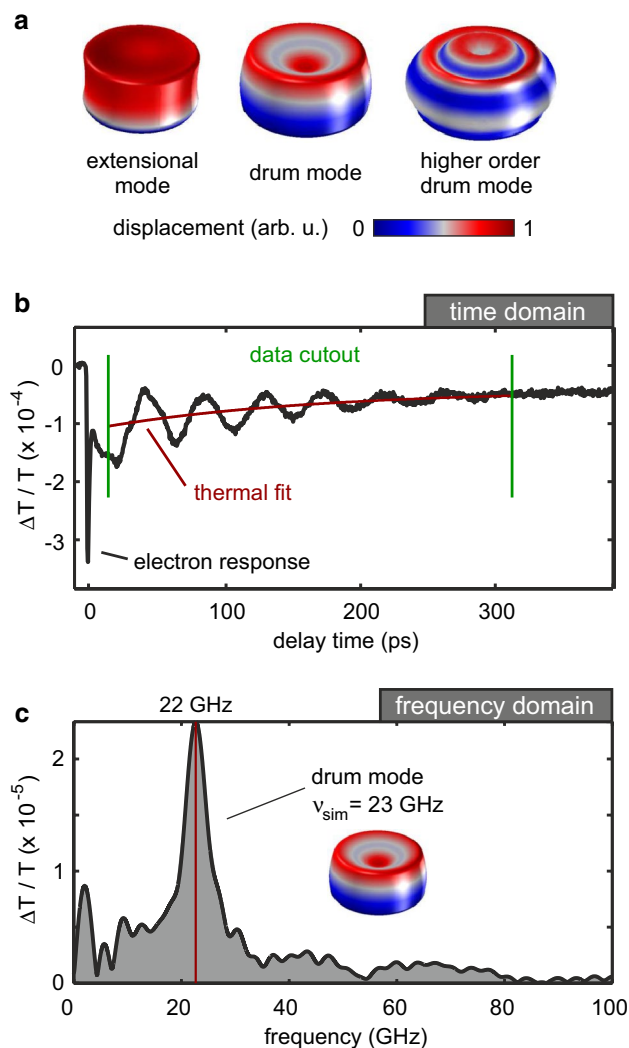

Fig. 4 *Ultrafast nonlinear response of a single gold nanoparticle* **a** Examples for mechanical modes of a disk-shaped gold nanoparticle, computed using a FEM solver. **b** The perturbation of the optical properties by the mechanical deformation leads to a transient nonlinear response. In order to analyze the bare oscillation signal, we cut out a region of interest (*green lines*) and subtract the thermal offset (*red curve*), fitted by a mono exponential function. **c** The contribution of the mechanical oscillation is separated and Fourier transformed, leading to the mechanical mode spectrum of the particle. The dominant mode at 22 GHz can be assigned to the drum mode by comparing the result of the numerical model at 23 GHz eigenfrequency

and a probe pulse wavelength of 635 nm. For further details concerning the experimental setup and parameters, we refer to a previous publication [12]. The measured time-dependent nonlinear response is given by the black curve in Fig. 4b. Directly after excitation at 0 ps, a short feature in the nonlinear response appears which is caused by the highly excited conduction band electrons [19]. On a picosecond timescale, energy of the hot electron gas is transferred to the lattice by electron-phonon scattering, until both are in thermal equilibrium [25]. This results in a slowly decaying thermal feature. Superimposed on this background, we find a decaying oscillation trace, caused by the mechanical oscillation that modulates the plasmon resonance of the nanoparticle [12, 15].

The mechanical spectrum (Fig. 4c) is determined by the Fourier transform of the bare oscillation trace. We find one mechanical mode at $\nu_{mech} \approx 22$ GHz, dominating the mechanical response between 0 and 100 GHz. In comparison, the prediction for the drum mode resonance by our numerical model is at $\nu_{sim} \approx 23$ GHz, in good agreement with the measurements. Furthermore, we study this result as a function of probe wavelength while the excitation is kept constant. Since the mechanical properties are independent of the optical measurement process, the drum mode resonance is not influenced and thus constant in frequency, amplitude, and decay. However, the signal amplitude has an optical origin and depends on the probe wavelength and plasmon resonance of the particle as shown in Fig. 5a. We model the full experiment, including optical excitation, mechanical and optical response, and optical detection. To this end, we employ a T-Matrix method [26] and compute the change of the particle's optical properties by combining the Drude model and a two-temperature model [12, 25]. The experimental data and our model are in good agreement as long as the d-band absorption of gold can be neglected, i.e., above approximately 600 nm wavelength.

To further check our numerical model that we want to use for the development of optimized antenna parameters, we investigate nanoparticles of different sizes, all 30 nm in height but with varying diameters between 40 and 90 nm. In order to fully predict the signal amplitude of the nonlinear response with our model, we have to consider both the interrogation (probe) process, which we discussed previously, but also the spectral dependence of the excitation (pump). One may expect the lattice temperature and the optical properties to be independent of the particle size as the increased absorption by a larger particle is canceled out by the larger volume that has to be heated. However, by increasing the disk diameter, the plasmon resonance shifts over the pump wavelength as illustrated in the inset of Fig. 5b. Consequently, the absorbed energy and also the excitation strength change,
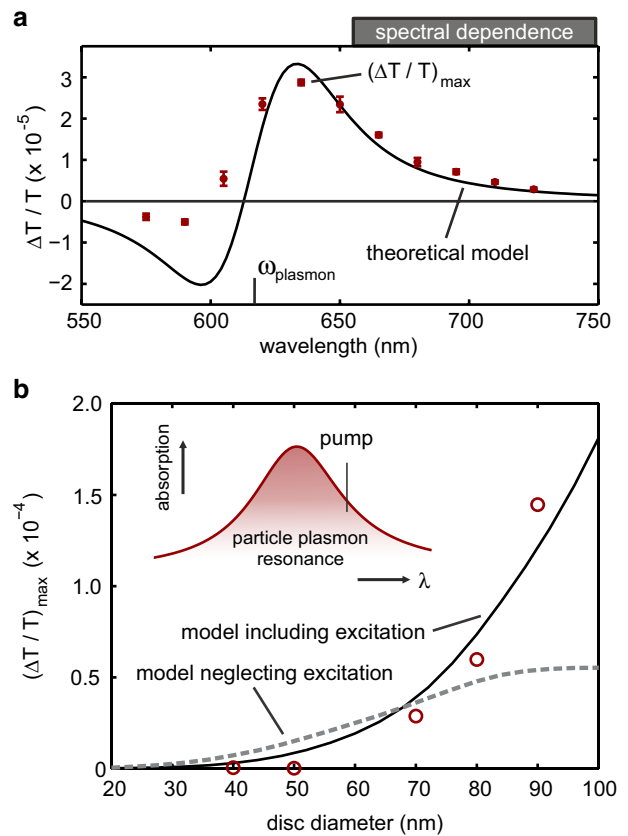

Fig. 5 *Probe wavelength and size-dependent response* **a** Signal amplitude of the mechanical mode at 22 GHz, extracted from the mechanical spectra of different probe wavelengths between 575 and 725 nm (*Symbols*) compared to a numerical model (*black curve*). For all measurements, the pump excitation is kept constant. The dispersive line shape is located around the particle plasmon resonance $\omega_{plasmon}$. **b** Signal amplitude of the mechanical mode as function of disk diameter. The excitation process has to be taken into account (*black solid curve*) as otherwise the strong increase in the signal cannot be explained (*dashed curve*)

as described by the two-temperature model. We now consider the pump as well as the previously discussed probe process. We find a good agreement between experiment and our model. The small deviations for the 40 and 50 nm disks (Fig. 5b) are due to their plasmon resonances below 600 nm and the neglected d-band perturbation in our simulations. A model ignoring the varying excitation conditions fails to match the measured data. We can thus apply our model to perform numerical optimization studies for this nanosystems.

In the described experimental configuration, our investigations are limited to nanoparticles with a diameter of 40 nm or larger, since the signal vanished for smaller particles in the shot noise of the probe beam. In order to measure the effect of the antenna in the strong scattering regime, we choose the 40 nm nanoparticle for our study. For simplicity, we first neglect the pump process

and consider the nonlinear response of the nanoparticle in the coupled system. Here, we tune the antenna diameter and search for the maximum nonlinear response for the case of a probe polarization along the long structure axis (Fig. 6a). As expected, the hybrid mode (ω^+ in Fig. 1) is red-shifted with respect to the single antenna. The corresponding nonlinear response has a maximum at an antenna diameter of about 70 nm (white cross in Fig. 6b). We keep in mind that this antenna is not yet optimized for the excitation process. However, we compute the energy of the pump pulse deposited in the nanoparticle and predict a three times higher excitation via the antenna. Consequently, we have an unoptimized excitation, giving us an enhancement by a factor of approximately 3, and an optimized antenna for the readout giving an additional enhancement factor of 2.5, leading to an overall antenna enhancement by almost one order of magnitude. To test these predictions, we study a coupled antenna–nanoparticle pair with a distance of 15 nm [12]. The antenna-enhanced response is compared with the maximum signal of 27 individually measured particles with 40 nm in diameter (Fig. 6c). We obtain a signal enhancement by approximately one order of magnitude. The experimental result even slightly surpasses the theoretical prediction as we neglected the d-band absorption in our simulations, hence overestimating the signal of the single nanoparticle, as shown in Fig. 5b. In the transient absorption spectrum (Fig. 6d), we find a redshift of the whole nonlinear response. This demonstrates that in the strong scattering regime the response of a small particle can be shifted out of the d-band absorption of gold, giving a large contribution to the signal enhancement even without the oscillator strength of the antenna.

Further numerical studies reveal the same counterintuitive behavior due to the optical properties of the antenna material, as previously discussed in our point-dipole model. We find that the most efficient antenna for a nanoparticle with twice the diameter (80 nm) is smaller and blue-shifted with respect to the nanoparticle itself.

The antenna structure can be optimized even further by efficiently exciting the nonlinear process. Unfortunately, an optimum antenna for the interrogation process is not necessarily the optimum for the excitation process due to the different spectral positions of pump and probe pulse. In order to optimize the excitation as well as the interrogation process, we suggest an L-type nanoantenna, as depicted in Fig. 7. Here, two antennas are arranged orthogonally to the nanoobject under investigation. By choosing different polarization of the excitation and probe pulse, both antennas can be optimized almost separately without disturbing each other by strong hybridization effects [27].
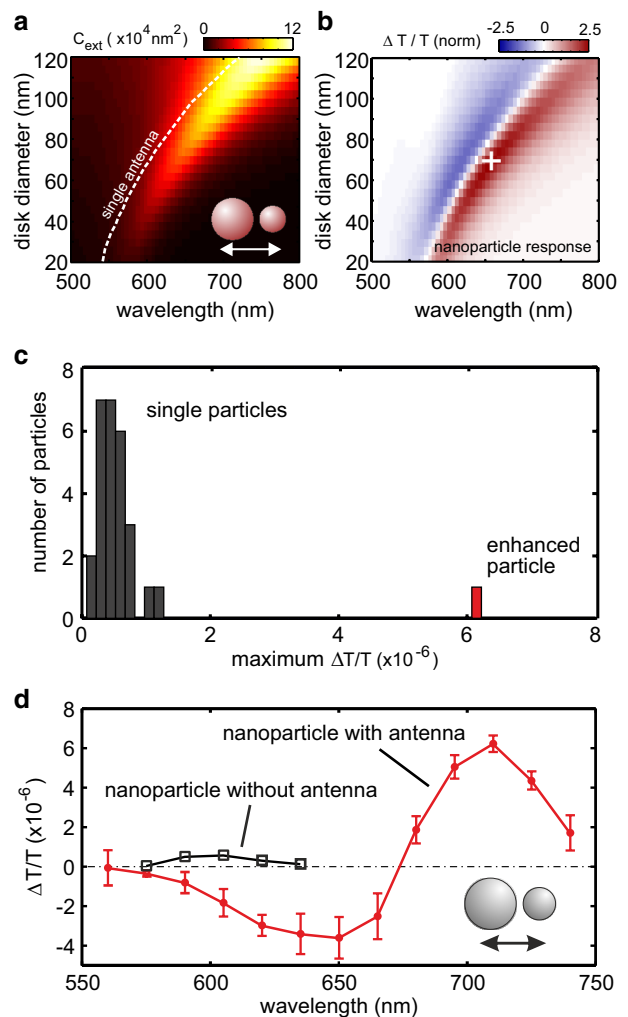

Fig. 6 *An antenna for mechanical breathing mode* **a** Linear extinction spectra of the coupled system, as a function of the antenna diameter. The distance between nanoparticle and antenna is kept constant at 10 nm. The hybrid mode is red-shifted compared to the resonance of the antenna alone (*white dashed curve*). **b** Nonlinear response of the hybrid system. The *white cross marks* the maximum nonlinear response. **c** In the experiment the antenna-enhanced particle gives a signal about a factor of 10 stronger than an ensemble of reference particles. **d** Transient absorption spectra of a single nanoparticle (*black curve*, *open symbols*) compared to the antenna–nanoparticle hybrid (*red curve*, *closed symbols*). The hybrid response is spectrally *red-shifted*, proving the strong scattering case and signal modulation to the hybrid mode at ω^+

4 The optimum antenna for carrier dynamics in a weakly scattering CdSe nanowire

In contrast to the previous example, we now consider the case of a weakly scattering nanoobject. For this purpose, we use the quantum-confined excitonic transitions in a single CdSe nanowire, recently investigated by ultrafast nonlinear spectroscopy [16, 28]. Figure 8 summarizes
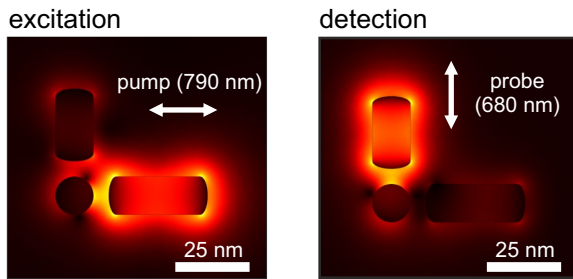
Fig. 7 *Optimized antennas* Complex antenna structure, consisting of two orthogonal antennas where one is optimized for pump excitation of the nanoparticle, the other one for detection enhancement
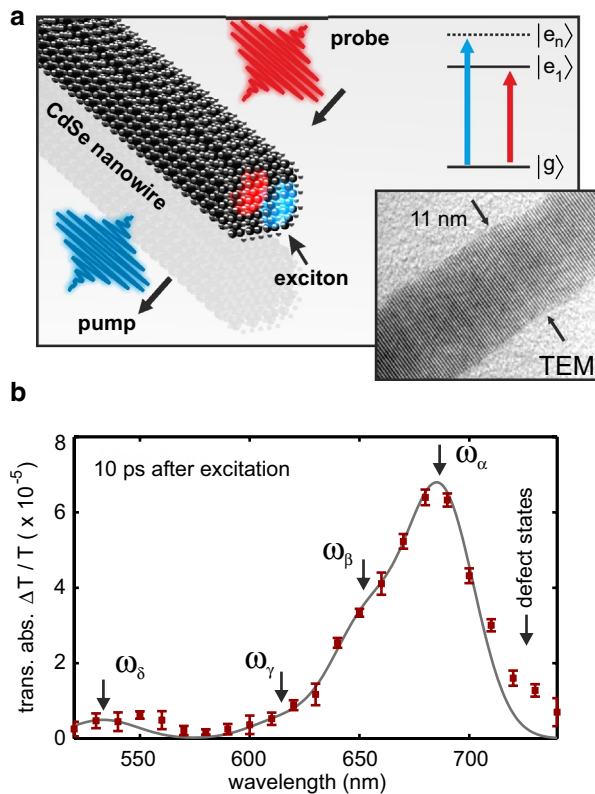

Fig. 8 *Quantum-confined carrier dynamics in a single CdSe nanowire* **a** Sketch of the experiment. A pump pulse at 390 nm excites an exciton into a quantum-confined state of a single CdSe nanowire, as illustrated in the ladder scheme. The probe pulse interrogates the temporal population of these states via their transition bleaching. *Inset* high-resolution TEM image of a typical wire, revealing small variations in the diameter along the wire. **b** Transient transmission spectrum, 10 ps after excitation. For the measured wire diameter of 11.6 nm, a six-band effective mass mode predicts dipole allowed transitions at $\omega_\alpha...\omega_\delta$, marked by the *black arrows*. The *gray curve* shows a fit of four Gaussian at these transition energies, all with a constant width and only the amplitude as free fit parameter

Fig. 9 *Optimizing the antenna for a weakly scattering nanoobject* **a** As model system, we consider a *disk-shaped* gold antenna with variable diameter, interacting with a spherical CdSe nanocrystal in center height and constant distance to the antenna surface. **b** Normalized nonlinear response of the coupled system as function of the antenna diameter. The *dashed curves* give the spectral position of the uncoupled antenna resonance and α-transition, respectively. The maximum nonlinear response is achieved with the antenna with 75 nm in diameter. **c** Nonlinear spectrum at the optimum antenna size (*black curve*). The *green dashed curve* shows 10 times the normalized nonlinear response of the bare nanocrystal, assumed to have the same spectral behavior as the wire of Fig. 8. The resonance of the bare gold antenna is plotted as *red curve* in arbitrary units, being resonant to the α-transition

leads to carrier confinement and discrete exciton states, deviating from the bulk band structure of CdSe [29, 30]. A 150 fs pump pulse at 390 nm wavelength excites the wire from the ground state $|g\rangle$ to a higher state $|e_n\rangle$. On an ultrafast timescale, the excitation can decay and populate lower energetic states. A tunable probe pulse (red arrow)

the essential parts of the experiment. The high-resolution transmission electron microscope (TEM) image in the inset shows a typical wire. The small diameter of around 11 nm
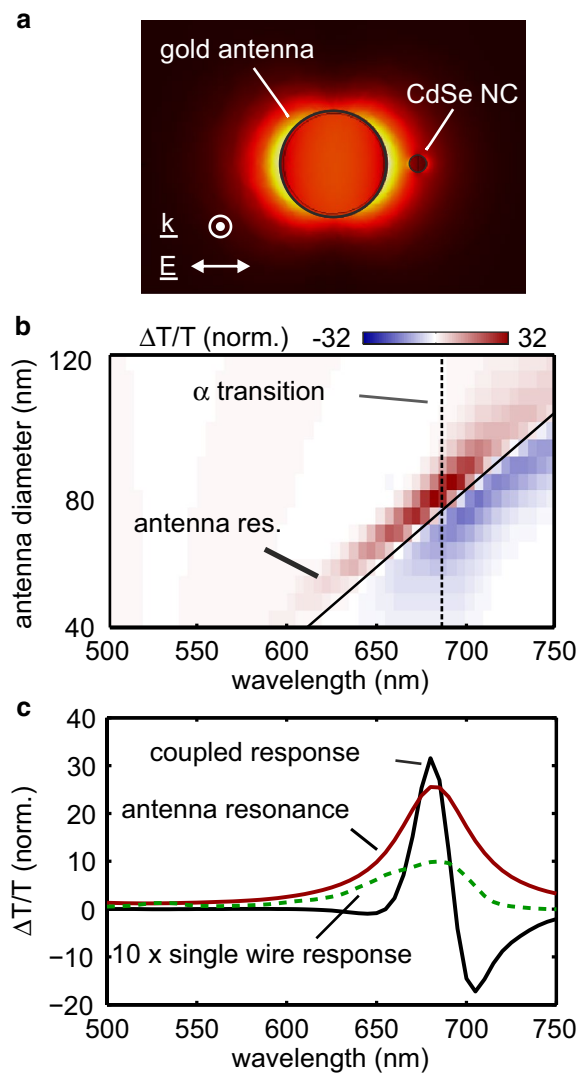
interrogates the optical response. At 10 ps after pump excitation, the relative increase in transmission $\Delta T/T$ reveals the pump-induced bleaching of four different transitions (Fig. 8b) which we label α to δ with corresponding transition energies ω_α to ω_δ. These transitions agree with energies obtained from a six-band effective mass model [29, 30] and are sufficient to describe the data below 720 nm wavelength (gray curve in Fig. 8b). The model fails for longer wavelengths, which we attribute to defects states. At this point, we refer to Ref. [16] for a more detailed discussion.

In analogy to the previous section, we want to study the coupling between a gold nanoantenna and a single CdSe nanowire. In order to optimize the antenna for this condition, we consider the model shown in Fig. 9a. For simplicity, the wire is replaced by a small spherical CdSe nanocrystal (NC) with 12 nm in diameter, placed into the near field hot spot 10 nm beside the gold antenna with 15 nm height. The nonlinear response of the NC is modeled by a Kramers–Kronig consistent modification of the complex dielectric function of bulk CdSe, imitating the bleaching measured previously. In our simulation, we

again tune the diameter of the antenna and investigate the predicted nonlinear response of the coupled system. The computed differential spectra (Fig. 9b) are normalized to the maximum nonlinear response of the single NC. We find the maximum nonlinear response for an antenna, which is resonant with the α-transition at approximately 690 nm wavelength. This corresponds to an antenna diameter of 75 nm. The predicted spectral behavior for this optimum antenna is plotted in Fig. 9c. It has a 32 times larger signal than the single nanocrystal. As expected, we find that the weak dipole moment of the nanocrystal does not shift the hybrid mode.

Finally, we experimentally study the influence of the antenna on a single CdSe nanowire with 12 nm diameter. Therefore, we couple an antenna array of ten equidistant gold nanodisks (height 15 nm, diameter 75 nm) to a CdSe nanowire (Fig. 10a). Our diffraction limited setup allows us to separately measure the two marked areas on the antenna–wire system, representing the spot sizes of the applied laser pulses. In this configuration, we are able to directly investigate the influence of the antenna on a single wire. A 5-nm
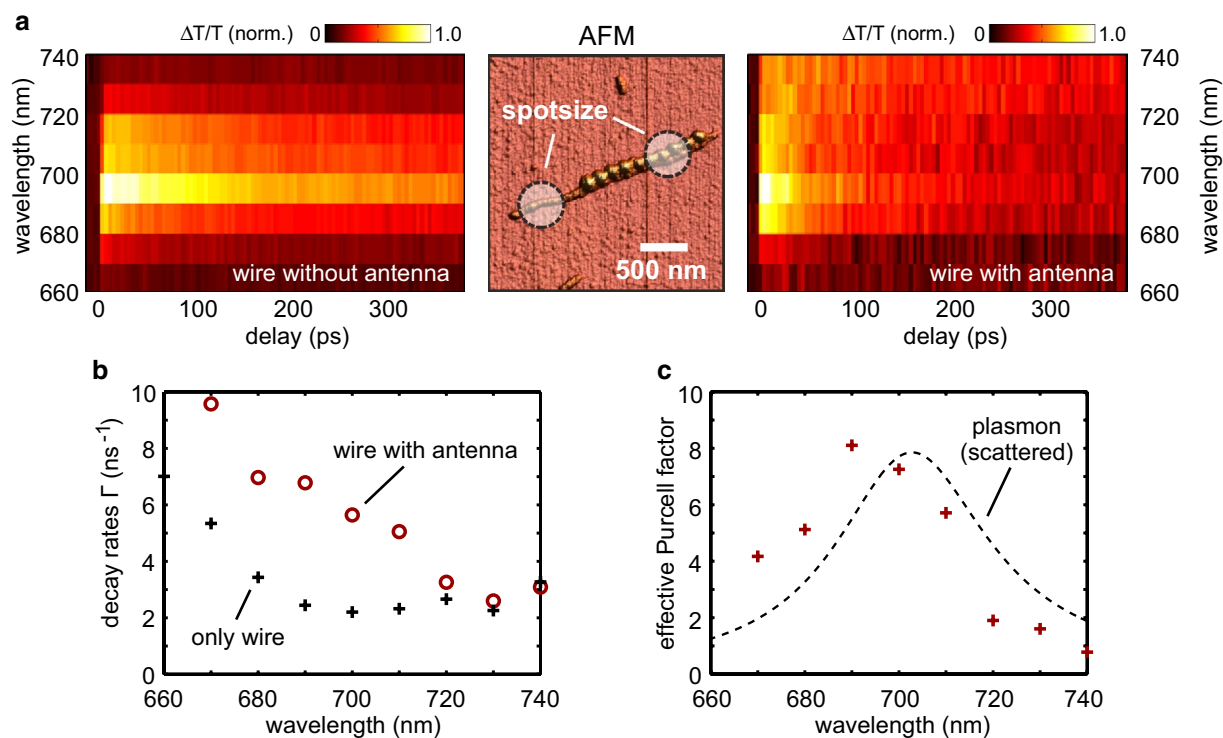

Fig. 10 *A plasmonic nanoantenna coupled to a CdSe nanowire* **a** In order to investigate the effect of the plasmonic nanoparticles, only a part of the wire is coupled to an antenna array as shown in the AFM image. The *circles mark* the investigated regions of the wire–antenna system. The normalized transient transmission spectra are measured over 400 ps in the spectral region of the α and β transition. In both cases, the pump and probe beam polarization is along the wire axis. The response of the uncoupled part (*left panel*) is similar to the single wire discussed before. The hybrid system (*right panel*) shows the same spectral behavior but with a decreased signal intensity and state lifetimes. **b** Decay rates of the bare wire (*black crosses*) and the coupled system (*red circles*), extracted from the data in (**a**) by fitting a single exponential function. **c** Effective Purcell factor (*symbols*) compared to a Lorentzian of the plasmon resonance (*black dashed curve*) obtained from dark-field scattering spectroscopy

layer of TiO_2, deposited on the wire by atomic layer deposition, avoids direct contact with the gold antenna array, which is written in a second step by electron beam lithography [31]. We measure a horizontal gap of 15 nm between the antenna structure and the wire. We limit ourselves to the α and β transitions and measure the response of the coupled and uncoupled wire. In addition, a single antenna array is investigated where we find no nonlinear response due to the weaker excitation power compared to the experiments above. The spectrally and time resolved response of the two areas are shown on the left (bare wire) and on the right side (coupled system) of Fig. 10a. In both cases, the transition energy and line width of the α-transition are in good agreement with the result of the wire studied previously. Furthermore, the hybrid response of antenna and wire is not detuned. The maximum transient response amplitude and lifetime of the uncoupled wire states do not change compared to the single wire experiment. This allows the conclusion that the experiment is not affected by the TiO_2 layer. However, the part coupled to the antenna exhibits strong changes of the decay time (Fig. 10b). While transitions at longer wavelengths seem to be almost unaffected by the antenna, the lifetime at around 690 nm wavelength is reduced by a factor of three. The plasmonic nanostructure increases the local density of states (LDOS), giving additional decay channels [32, 33]. A common value to describe this phenomenon is the effective Purcell factor, given by

$$P_{\text{eff}} = \frac{\Gamma_{\text{rad,c}}}{\Gamma_{\text{rad,0}}} = \frac{\Gamma_{\text{tot,c}}/\Gamma_{\text{tot,0}} - 1 + \eta_Q}{\eta_Q} \qquad (6)$$

with $\Gamma_{\text{rad,}c}$ being the radiative decay rate of the coupled system, $\Gamma_{\text{rad,0}}$ of the uncoupled system. Furthermore, P_{eff} can be expressed by the ratio of the absolute decay rates $\Gamma_{\text{tot,}c}$ and $\Gamma_{\text{tot,0}}$ and the quantum efficiency η_Q of the nanocrystal, which we determined to 0.25 [16]. The result is plotted in 10c. As the decay of each excitonic state depends on the local density of states, the lifetimes and thus the Purcell factors differ for the different transitions and wavelengths. We find back the plasmon resonance in both the decay rate increase and Purcell factor. The absorption resonance is slightly blue-shifted with respect to the scattering response. Consequently, the α-transition, which is resonant with the antenna, shows a Purcell factor of 8. The Purcell factor around the β-transition is approximately 5. The Purcell factor of the defect states, located at higher wavelength, is almost one as the antenna is off-resonant there.

However, the predicted signal enhancement is not observed. Comparing the maximum response of the uncoupled and coupled wire, we find a signal decrease to 1/3 for the antenna–wire hybrid. We explain this by the rough approximation with the spherical nanocrystal that we assumed in our simulations. While the near field of the antenna increases the light–matter interaction in the whole nanocrystal, leading to a

strong signal enhancement, large areas of the wire are not or even negatively influenced by the antenna. Furthermore, we had to choose the probe polarization along the wire axis to resolve the linear response of the wire, reducing the antenna efficiency since the near field at the wire's position is drastically reduced. However, although the nonlinear response is not enhanced, we find interaction between the nanowire and antenna by the increased local density of states revealed by the enormous increase in the decay rate. Furthermore, we find that the antenna is not detuned by the weakly scattering nanowire, supporting our numerical study.

5 Conclusion

To summarize, we theoretically and experimentally demonstrated that optical nanoantennas are a powerful tool to increase the light–matter interaction in a sub-diffraction limited area. In dependence of the feedback on the antenna, we distinguish between strongly and weakly scattering nanosystems. While the spectral influence of the weakly scattering nanoobject on the antenna resonance can be almost neglected, the feedback of the strong scatterer detunes the hybrid mode with respect to the antenna resonance. We introduced and applied a point-dipole model based on the discrete dipole approximation, to simplify the huge parameter space and study the correlation between the optimum antenna and nanosystem resonance. We find that the dielectric properties of the antenna are a crucial parameter for maximum signal enhancement. In the case of the strong scattering nanosystem, the antenna can be used to shift the hybrid response into spectral regions with beneficial optical properties. Here, even an off-resonant antenna can enhance the nanosystem's nonlinear response by its additional oscillator strength. For the weakly scattering nanosystem, the optimum antenna has to be in resonance. However, the optical properties of the antenna material limits the efficient spectral workspace of the optical nanoantenna. These findings were supported by two examples. In the case of the strongly scattering nanoparticle, we achieved a signal enhancement by one order of magnitude, by increasing the excitation as well as the interrogation process by an antenna. For the weakly scattering CdSe nanowire, we fond strong interaction between antenna and nanosystem but no signal enhancement until now.

References

1. A. Alivisatos, Semiconductor clusters, nanocrystals, and quantum dots. Science **271**(5251), 933–937 (1996)

2. J.A. Fan, C. Wu, K. Bao, J. Bao, R. Bardhan, N.J. Halas, V.N. Manoharan, P. Nordlander, G. Shvets, F. Capasso, Self-assembled plasmonic nanoparticle clusters. Science **328**(5982), 1135–1138 (2010)

3. W.E. Moerner, M. Orrit, Illuminating single molecules in condensed matter. Science **283**(5408), 1670–1676 (1999)

4. P. Bharadwaj, B. Deutsch, L. Novotny, Optical antennas. Adv. Opt. Photonics **1**, 438–483 (2009)

5. H. Harutyunyan, G. Volpe, R. Quidant, L. Novotny, Enhancing the nonlinear optical response using multifrequency gold-nanowire antennas. Phys. Rev. Lett. **108**, 217403 (2012)

6. P. Mühlschlegel, H.J. Eisler, O.J.F. Martin, B. Hecht, D.W. Pohl, Resonant optical antennas. Science **308**(5728), 1607–1609 (2005)

7. J. Butet, J. Duboisset, G. Bachelier, I. Russier-Antoine, E. Benichou, C. Jonin, P.F. Brevet, Optical second harmonic generation of single metallic nanoparticles embedded in a homogeneous medium. Nano Lett. **10**(5), 1717–1721 (2010)

8. M. Lippitz, M. van Dijk, M. Orrit, Third-harmonic generation from single gold nanoparticles. Nano Lett. **5**(4), 799–802 (2005)

9. N. Liu, M.L. Tang, M. Hentschel, H. Giessen, A.P. Alivisatos, Nanoantenna-enhanced gas sensing in a single tailored nanofocus. Nat. Mater. **10**(8), 631–636 (2011)

10. A. Kinkhabwala, Z. Yu, S. Fan, Y. Avlasevich, K. Muellen, W.E. Moerner, Large single-molecule fluorescence enhancements produced by a bowtie nanoantenna. Nat. Photonics **3**(11), 654–657 (2009)

11. M. Pfeiffer, K. Lindfors, C. Wolpert, P. Atkinson, M. Benyoucef, A. Rastelli, O.G. Schmidt, H. Giessen, M. Lippitz, Enhancing the optical excitation efficiency of a single self-assembled quantum dot with a plasmonic nanoantenna. Nano Lett. **10**(11), 4555–4558 (2010)

12. T. Schumacher, K. Kratzer, D. Molnar, M. Hentschel, H. Giessen, M. Lippitz, Nanoantenna-enhanced ultrafast nonlinear spectroscopy of a single gold nanoparticle. Nat. Commun. **2**, 333 (2011)

13. V. Myroshnychenko, J. Rodriguez-Fernandez, I. Pastoriza-Santos, A.M. Funston, C. Novo, P. Mulvaney, L.M. Liz-Marzan, F.J. Garcia de Abajo, Modelling the optical response of gold nanoparticles. Chem. Soc. Rev. **37**(9), 1792–1805 (2008)

14. K. Kelly, E. Coronado, L. Zhao, G. Schatz, The optical properties of metal nanoparticles: the influence of size, shape, and dielectric environment. J. Phys. Chem. B **107**(3), 668–677 (2003)

15. M.A. van Dijk, M. Lippitz, M. Orrit, Detection of acoustic oscillations of single gold nanospheres by time-resolved interferometry. Phys. Rev. Lett. **95**(26), 267406 (2005)

16. T. Schumacher, H. Giessen, M. Lippitz, Ultrafast spectroscopy of quantum confined states in a single CdSe nanowire. Nano Lett. **13**(4), 1706–1710 (2013)

17. S.S. Lo, T.A. Major, N. Petchsang, L. Huang, M.K. Kuno, G.V. Hartland, Charge carrier trapping and acoustic phonon modes in single CdTe nanowires. ACS Nano **6**(6), 5274–5282 (2012)

18. M. Perner, S. Gresillon, J. Marz, G. von Plessen, J. Feldmann, J. Porstendorfer, K.J. Berg, G. Berg, Observation of hot-electron pressure in the vibration dynamics of metal nanoparticles. Phys. Rev. Lett. **85**(4), 792–795 (2000)

19. J. Bigot, V. Halte, J. Merle, A. Daunois, Electron dynamics in metallic nanoparticles. Chem. Phys. **251**(1–3), 181–203 (2000)

20. B. Draine, P. Flatau, Discrete-dipole approximation for scattering calculations. J. Opt. Soc. Am. A Opt. Image Sci. Vis. **11**(4), 1491–1499 (1994)

21. E. Prodan, C. Radloff, N.J. Halas, P. Nordlander, A hybridization model for the plasmon response of complex nanostructures. Science **302**(5644), 419–422 (2003)

22. P.B. Johnson, R.W. Christy, Optical constants of noble metals. Phys. Rev. B **6**(12), 4370–4379 (1972)

23. J.H. Hodak, A. Henglein, G.V. Hartland, Size dependent properties of au particles: coherent excitation and dephasing of acoustic vibrational modes. J. Chem. Phys. **111**(18), 8613–8621 (1999)

24. *Comsol Multiphysics structural mechanics—user's guide*. Comsol 2012, version: 4.3

25. G.V. Hartland, Coherent excitation of vibrational modes in metallic nanoparticles. Annu. Rev. Phys. Chem. **57**, 403–430 (2006)

26. A. Doicu, T. Wriedt, Y. Eremin, *Light Scattering by Systems of Particles. Null-Field Method with Discrete Sources—Theory and Programs* (Springer, Berlin, 2006)

27. A.M. Funston, C. Novo, T.J. Davis, P. Mulvaney, Plasmon coupling of gold nanorods at short distances and in different geometries. Nano Lett. **9**(4), 1651–1658 (2009)

28. C. Carey, Y. Yu, M. Kuno, G. Hartland, Ultrafast transient absorption measurements of charge carrier dynamics in single II–VI nanowires. J. Phys. Chem. C **113**(44), 19077–19081 (2009)

29. J. Giblin, F. Vietmeyer, M.P. McDonald, M. Kuno, Single nanowire extinction spectroscopy. Nano Lett. **11**(8), 3307–3311 (2011)

30. A. Shabaev, A.L. Efros, 1D Exciton spectroscopy of semiconductor nanorods. Nano Lett. **4**(10), 1821–1825 (2004)

31. M. Pfeiffer, K. Lindfors, P. Atkinson, A. Rastelli, O.G. Schmidt, H. Giessen, M. Lippitz, Positioning plasmonic nanostructures on single quantum emitters. Phys. Status Solidi (b) **249**(4), 678–686 (2012)

32. P. Anger, P. Bharadwaj, L. Novotny, Enhancement and quenching of single-molecule fluorescence. Phys. Rev. Lett. **96**(11), 113002 (2006)

33. J. Goffard, D. Gerard, P. Miska, A.-L. Baudrion, R. Deturche, J. Plain, Plasmonic engineering of spontaneous emission from silicon nanocrystals. Sci. Rep. **3**, 2672 (2013)